Journal of
Ceramic Science
and Technology

J. Ceram. Sci. Tech., **05** [04] 309-316 (2014)
DOI: 10.4416/JCST2014-00014
available online at: http://www.ceramic-science.com
© 2014 Göller Verlag

Performance and Stability of Mixed Conducting Composite Membranes Based on Substituted Ceria

U. Pippardt*[1], J. Böer[1], Ch. Bollert[1], A. Hoffmann[1], M. Heidenreich[2], R. Kriegel[1], M. Schulz[1], A. Simon[2]

[1]Fraunhofer Institute for Ceramic Technologies and Systems IKTS, Michael-Faraday-Str. 1, D-07629 Hermsdorf, Germany
[2]Bauhaus-University Weimar, Coudraystrasse 13C, D-99423 Weimar, Germany
received April 14, 2014; received in revised form June 6, 2014; accepted July 5, 2014

Abstract

High-temperature dual-phase oxygen separation membranes were successfully prepared from different $Ce_{0.8}Gd_{0.2}O_{2-\delta}$ (CG)-spinel mixtures according to the mixed oxide route. $MnCo_{1.9}Fe_{0.1}O_4$ (C19) and $Cu_{0.6}Ni_{0.4}Mn_2O_4$ (M2) were used as the spinel components with volume fractions of 10, 20, 30, 40 and 50 vol% respectively. The formation of an electron-conducting percolative network by the spinel components was investigated based on electrical resistivity measurements at room temperature. The oxygen permeation behaviour of the composites was determined as a function of the material composition and the temperature. The highest oxygen flux of approximately 0.14 ml (STP)/cm²min was obtained with samples of 0.8 mm thickness at 900 °C and a spinel content of 30 vol%. The stability of the individual phases was proven by means of X-ray-diffraction (XRD) and microstructural investigations after sintering and high-temperature exposure experiments at 850 °C in a CO_2- and SO_2-containing model flue gas. No degradation of the composite materials was observed. However, semi-long-term permeation experiments in an air/CO_2 gradient revealed a strong increase of the oxygen flux as a function of time accompanied by intensive material corrosion probably caused by kinetic demixing.

Keywords: Oxygen separation, mixed conductor, CO_2 stability, composites, ceria

I. Introduction

Oxygen separation using MIEC (Mixed Ionic Electronic Conductor) membranes at high temperatures has been identified as an energy-efficient alternative to mature cryogenic air separation for oxyfuel combustion of coal in power plants [1]. Recently published values for the specific energy consumption vary between 160 and 340 kWh/t O_2 depending on optimization of the cryogenic plant, on the degree of integration into a power plant [2], but also on plant size [3]. Nevertheless, the membrane process integrated in a coal power plant should be able to reach much lower energy consumption between 94 and 26 kWh/t O_2 especially for a high degree of integration in a so-called 4-end operation mode [4] using flue gas for sweeping.

MIEC membrane materials with high oxygen permeation are usually based on the perovskite structure type ABO_3 containing high amounts of alkaline earths reacting with flue gas components like CO_2 [5,6] and SO_2 [7] entailed by a reversible or permanent blocking of the O_2 permeation. Different attempts to stabilize high-flux MIEC have been conducted either by substitution on the A site by Ca [8] or on the B site by Ti [9] and Nb [10] or by testing alkaline-earth-free compositions [11]. As a result, a slow decline of the O_2 permeation as a function of time has been determined for partially substituted Co-containing perovskites in long-term permeation measurements [12]. Carbonation stability but a much lower O_2 permeation using a CO_2 sweep gas has been found for $Ca_{0.5}Sr_{0.5}Fe_{0.2}Mn_{0.8}O_{3-\delta}$, $La_2NiO_{4+\delta}$ and for a metallic-silver-infiltrated $Ce_{0.8}Sm_{0.2}O_{2-\delta}$ [12]. The latter is expected to be stable in CO_2 and in SO_2.

It is already known that metallic silver tends to sublimate at high temperatures, especially at low pressure. Therefore, it was meaningful to substitute the electronic conducting phase (ECP) with oxides that tolerate the abovementioned gases. Corresponding to the related operation conditions for oxygen permeation and for SOFC, different electrode materials were evaluated regarding possible reactive components and long-term conductivity performance. According to [13], two spinel compositions were selected as ECP for the MIEC composites.

II. Experimental

(1) Sample preparation

A commercial $Ce_{0,8}Gd_{0,2}O_{2-\delta}$ (CG) powder (Treibacher Industry AG) was used as ionic conductive phase. The average grain size of 200 nm and the phase composition was confirmed with SEM and XRD, respectively.

The spinel compositions $MnCo_{1.9}Fe_{0.1}O_4$ (C19) and $Cu_{0.6}Ni_{0.4}Mn_2O_4$ (M2) were prepared by means of solid

* Corresponding author: ute.pippardt@ikts.fraunhofer.de

state reaction using stoichiometric mixtures of $CuCO_3$, $CoCO_3$ (Chempur), Fe_2O_3 (HP-TKS), $MnCO_3$ (Riedel de Häen) and NiO (Merck, Selectipur). The powder mixtures were mixed and wet-milled in ethanol (technical grade) in a zirconia ball mill for 1 h. The slurry was dried at 80 °C and calcined at 1100 °C in air for 2 h in order to yield the phase formation of the spinels. After calcination, the powders were milled for 6 h in ethanol with zirconia grinding balls in a bead mill. After milling, the spinel powders were characterized with BET (ASAP 2020, Micro-Meritics). The BET surface was determined at 13.67 m²/g for C19 and 14.63 m²/g for M2. The phase structure of the spinels was studied by means of X-ray diffraction (XRD, D8 Advance, Bruker AXS, $Cu_{K\alpha}$ radiation) and will be discussed later.

Composite membrane samples with different volume fractions of the CG- and the spinel phases were prepared as summarized in Table 1. After they had been weighed, the powders were mixed for 20 h in ethanol in a grinding drum with zirconia balls. Subsequently, the powders were dried at 60 °C, granulated through a 315-μm sieve and pressed uniaxially to discs with a diameter of 18 mm in a hydraulic press at a pressure of 31 MPa. The samples were sintered at different temperatures between 1100 °C and 1300 °C with 2 h dwell time applying a heating rate of 5 K/min. To prove defect-free and gas-tight samples, the open porosity of the sample discs was determined by means of Hg-intrusion porosimetry (Pascal 140/440, Porotec). The open porosity amounted to 0.5 vol% for CG/C19 composites and to 1.5 vol% for CG/M2. After they had been sintered, the solid pellets were polished to achieve plane-parallel surfaces with a sample thickness of approximately 0.8 mm.

(2) Thermal expansion behaviour

The measurement of the thermal expansion coefficient (TEC) was conducted in the range from 20 °C to 1000 °C with a heating rate of 2 K/min using a dilatometer (L57HD from Linseis, Selb, Germany) in air. The TEC values of pure CG, M2, C19, 70:30 vol% mixtures as well as of $Ba_{0.5}Sr_{0.5}Co_{0.8}Fe_{0.2}O_{3-\delta}$ (BSCF5582) [14] for comparison, were calculated following the definition $\Delta l/l_0$ and the temperature.

(3) Oxygen permeation experiments

Oxygen permeation measurements were conducted using a high-temperature test rig already described by Kriegel *et al.*[12]. Temperatures of 600, 700, 800 and 900 °C were typically realized with ramps of 5 K/min and a dwell time of 2 hours at each temperature. Nitrogen (5.0) was used as sweep gas while the feed gas side was purged with dried air. The flow rates of the gases were set to 1000 ml (STP)/min at the feed side and to 169 ml (STP)/min on the sweep side (Q_{sweep}). All gas flows were regulated with mass flow controllers calibrated to standard conditions (1 bar, 273 K). For measuring the oxygen content of the sweep gas before p_{l_in} and after passing p_l the membrane, a customized two-channel zirconia-based analyzer manufactured by ZIROX® was used. The primary experimentally determined oxygen flux $j_{O2,exp}$ was calculated using the following equation where p_{abs} is the absolute pressure of 1 bar and A_M is the membrane area in cm².

$$j_{O_2,exp} = \frac{(p_l - p_{l\_in}) \cdot Q_{sweep}}{A_M \cdot (p_{abs} - p_l)} \quad (1)$$

$j_{O_2,exp}$ – measured oxygen flux, p_l – oxygen partial pressure in sweep gas after membrane contact, p_{l_in} – oxygen partial pressure in sweep gas before membrane contact, Q_{sweep} – throughput of the sweep gas before membrane contact at the gas inlet, A_M – membrane area, p_{abs} – absolute pressure of the sweep gas.

Table 1: Prepared material compositions

Declaration	Composition		
	$Ce_{0.8}Gd_{0.2}O_{2-\delta}$ **(CG)** [vol%]	$MnCo_{1.9}Fe_{0.1}O_4$ **(C19)** [vol%]	$Cu_{0.6}Ni_{0.4}Mn_2O_4$ **(M2)** [vol%]
CG/M2 – 90/10	90	-	10
CG/M2 – 80/20	80	-	20
CG/M2 – 70/30	70	-	30
CG/M2 – 60/40	60	-	40
CG/M2 – 50/50	50	-	50
CG/C19 – 90/10	90	10	-
CG/C19 – 80/20	80	20	-
CG/C19 – 70/30	70	30	-
CG/C19 – 60/40	60	40	-
CG/C19 – 50/50	50	50	-

The sample was mounted by clamping it between two recipients without any high-temperature sealing. Therefore, the experimental results had to be corrected with reference to the inaccuracies caused by leakages $j_{O_2,leakage}$ and the oxygen flux through the cylindrical shell surface of the sample discs $j_{O_2,shell}$. The final oxygen flux j_{O_2} was calculated according to Eq. 2.

$$j_{O_2,exp} = j_{O_2,exp} - (j_{O_2,shell} + j_{O_2,leakage}) \quad (2)$$

j_{O2} – corrected oxygen flux, $j_{O_2,shell}$ – additional oxygen flux through the cylindrical surface shell of the membrane sample, $j_{O_2,leakage}$ -oxygen introduced by leakages

The determination of the two leakage components have already been described in detail in previous work [12]. Owing to the low oxygen fluxes of the investigated materials, minimization of the stochastic errors from leakages was essential for correct results. Thus, much emphasis was placed on precise sample preparation by means of grinding and polishing as well as the accurate application of the sample in the test rig. As a typical result, all leakages measured at room temperature before and after each sample run were below 2.2 % of the oxygen flux reached at 900 °C. The mean value of all samples was 1.61 %.

In addition to the heat treatment investigations in model flue gas, the CO_2-stability of the composites was established in oxygen permeation tests with CO_2 (4.5) as a sweep gas applied for 75 h at 900 °C. CO_2 was typically applied after a standard measurement by switching from nitrogen to CO_2 at 900 °C.

(4) Resistivity measurement

Measurements of the electrical resistance were conducted simply with a two-point-conductivity meter at room temperature. The purpose was the detection of a possible disruption of the electronic conductive pathways at low contents of the ECP. The CG/M2- and CG/C19-samples with different spinel contents of 10, 20, 30, 40 and 100 vol% were contacted on both planar surfaces with a silver conductive paste. After drying, the sample discs were clamped in a specimen holder and electrically contacted via a defined spring force. The specific resistivity ϱ was calculated according to Ohm's law (Eq. 3).

$$\rho = \frac{R \cdot A}{l} \quad (3)$$

R: absolute resistance; A: surface area; l: sample thickness

(5) Heat treatment in a model flue gas atmosphere

The chemical stability of the composite samples was tested in a TGA unit (Deutsche Montan-Technologie Gesellschaft für Forschung und Prüfung, Essen mbH) which is shown schematically in Fig. 1. The appropriate model flue gas consisted of 95 vol% CO_2, 5 vol% O_2 and 400 ppm SO_2 (Air Liquide) and was chosen to realize an atmosphere close to conditions proposed by OXYCOAL-AC [15]. The dwell time varied between 5 and 24 h for powder samples and was set to 24 h for solid pellets at a constant temperature of 850 °C.

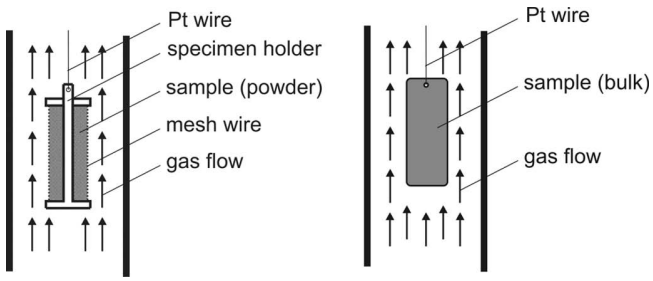

Fig. 1: Schematic showing the setup of the sample inside the TGA unit used for exposure corrosion tests; (left) for powder samples, (right) for bulk samples.

The gas-treated powder samples were characterized by means of X-ray diffraction (XRD) using a 3003 TT manufactured by Seifert. CuK_α-radiation in Bragg-Brentano geometry was used for measurements within a 2θ range from 22 to 140 °. The bulk samples were investigated applying identical parameters using a Seifert FOX XRD equipped with a focusing capillary optic for the primary beam together with a position-sensitive detector.

III. Experimental Results

(1) Powder and bulk characterization and phase formation

The XRD patterns of the CG and the prepared spinel powders after calcination at 1100 °C are shown in Fig. 2 and Fig. 3. As expected, the CG powder as well as the prepared spinel powders show single phases after calcination.

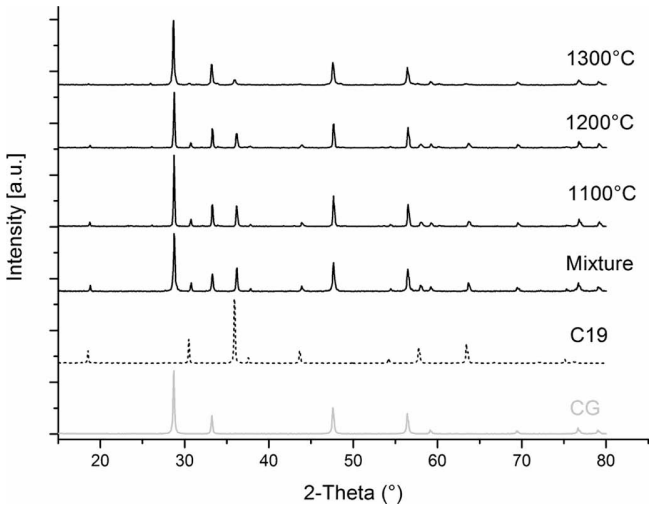

Fig. 2: XRD patterns of CG and the C19-spinel after calcination at 1100 °C and of the CG/C19 – 70/30 composite after mixing and heat treatment at different temperatures for 10 h each.

The X-ray diffractograms of the composites CG/C19 – 70/30 and CG/M2 – 70/30 are also shown in Fig. 2 and Fig. 3 after different thermal treatments for 10 h each. Up to temperatures of 1300 °C both phases (spinel and CG) coexist separately inside the composite material. Nevertheless, first appearances of the reaction between the two components at 1300 °C were found characterized by lowered intensities or disappeared reflexes of the spinel phase. This indicates that the composite materials are not stable at temperatures above 1200 °C.

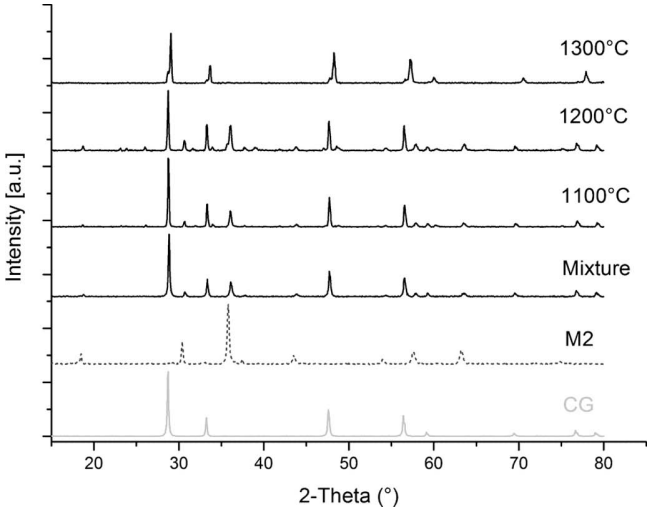

Fig. 3: XRD patterns of CG and the M2-spinel after calcination at 1100 °C and of the CG/M2 – 70/30 composite after mixing and heat treatment at different temperatures for 10 h each.

SEM analyses of the 70/30 composite materials sintered at 1200 °C are shown in Fig. 4. A homogeneous distribution of the spinel phase (represented by the grey components) was reached both for the M2- containing composite (left) and for the C19-composite (right). Additionally, a small amount of residual porosity is visible. The difference regarding the microstructure of the two composite materials is caused by the different particle size distributions of the starting powders (see Chapter II.(1)) and also by the different sintering activities of the materials.

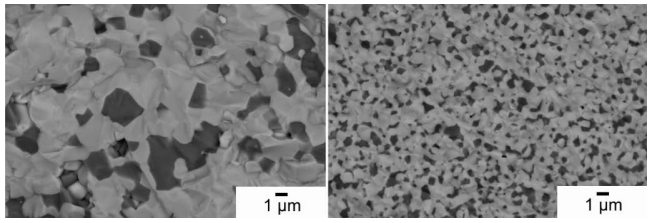

Fig. 4: SEM analysis of the composite materials after sintering at 1200 °C, (left) CG/M2 – 70/30 and (right) CG/C19 – 70/30.

(2) Thermal expansion behaviour

Fig. 5 shows the thermal expansion behaviour of the investigated 70/30 composite materials in comparison to CG and BSCF5582 as a typical representative for mixed conducting perovskites. There is only a low thermal mismatch between CG and C19 (left). Furthermore, curve linearity can be found instead of the non-linear behaviour of BSCF5582. The linear thermal expansion of the spinel C19 and a CG/C19 – 70/30 composite indicates the absence of chemically induced expansion. Therefore, the use of such a composite seems to be promising for asymmetric membranes supported by an inert porous material. For instance, magnesia exhibits a thermal expansion coefficient of $13 \cdot 10^{-6}$ K^{-1} matching the composite materials summarized in Table 2, although, the pure M2 spinel shown in Fig. 5 (right) is characterized by non-linear expansion behaviour. The observed increase in expansion above 500 °C could be explained by an oxygen release which results in chemical expansion. Nevertheless, this anomaly seems to be suppressed in the mixtures of CG and M2. The resulting expansion behaviour is close to the pure CG material.

Table 2: Thermal expansion coefficients of selected materials

Material	a_{1000} [$10^{-6}/K^{-1}$]
BSCF 5582	18.9
CG82	14.3
CG-C19	12.2
C19	11.9
M2	21.4
CG-M2	11.4
MgO	13.0

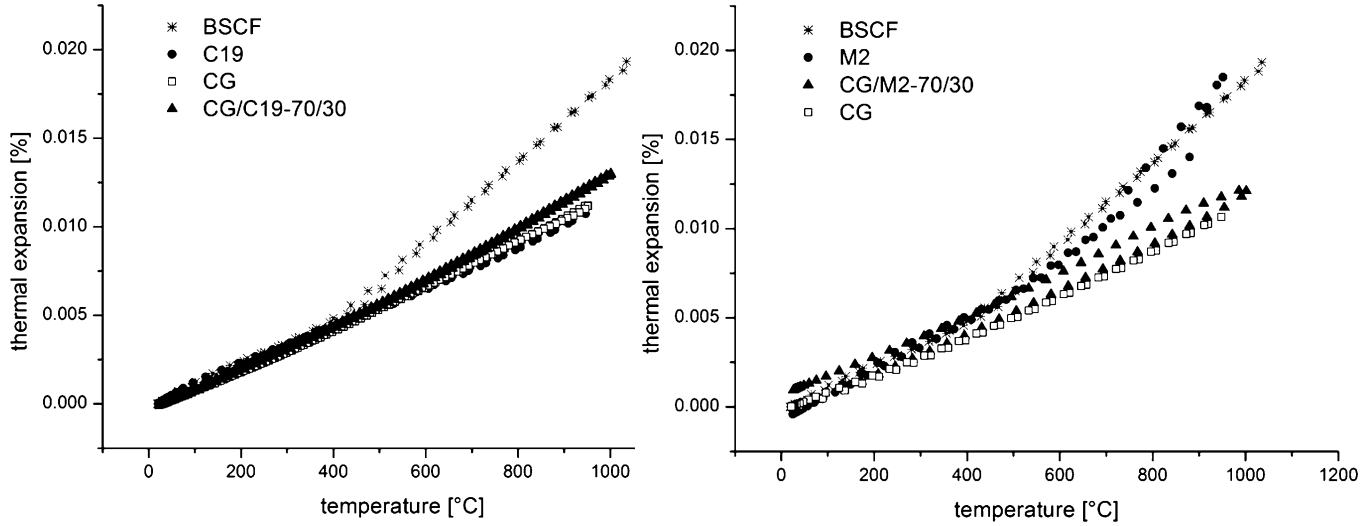

Fig. 5: Thermal expansion behavior of CG/C19 – 70/30 and C19 (left) and CG/M2 – 70/30 and M2 (right) in comparison to CG and BSCF.

(3) Electrical resistivity depending on volume fraction of components and formation of a percolative mixed conducting network

Pure CG exhibits very small electronic conductivity under standard conditions. The addition of a defined amount of the ECP to a composite material causes an abrupt rise of the ambipolar conductivity based on the formation of a percolative network, resulting in MIEC properties. To determine the percolation, threshold measurements based on the electric resistivity of the composite at room temperature were conducted. The measurements were conducted with three samples of the same composition. The experimental electric resistivity is plotted against the ECP content in Fig. 6. The resistivity decreases with increasing spinel content. A disproportionate decrease of the electric resistivity is visible already at 20 vol% of both ECPs, which provides evidence for increasing formation of percolative pathways. A bond percolation model (see e.g. the critical thresholds for f.c.c. packages [17]) was used to describe the resistivity as a function of the ECP content as represented by the dashed lines in Fig. 6.

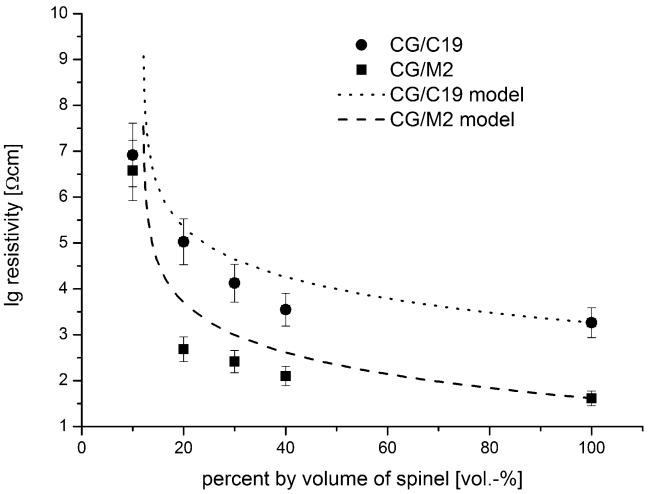

Fig. 6: Electric resistivity plotted against the spinel content (symbols) and calculated resistivities according to the percolation model by [16] and [17](dashed lines).

(4) Oxygen permeation

All prepared samples were tested for oxygen permeation in the as-described test rig in an air/nitrogen gradient within a temperature range from 600 to 900 °C. The sample thickness of 0.8 mm was held constant for all measurements. Therefore, it is possible to compare the measured results directly without any normalization. The oxygen flux at 900 °C is plotted in Fig. 7 for both composite materials vs. the ECP volume fraction. The oxygen flux values scatter across a low range between 0.06 up to 0.14 ml (STP)/cm²min. The content of the electronic conducting spinel phase exerted a significant influence on the oxygen flux.

An oxygen flux of approximately 0.07 ml (STP)/cm²min was observed for CG/M2 at a high ECP fraction of 50 vol%. A decreasing content of the spinel phase is accompanied by increasing oxygen fluxes up to 0.14 ml (STP)/cm²min at 30 vol% ECP. After exceeding this maximum, the oxygen flux decreases. A similar behaviour was observed for the CG/C19 composite with a slight shift of the highest oxygen flux to a lower ECP content of only 20 vol%.

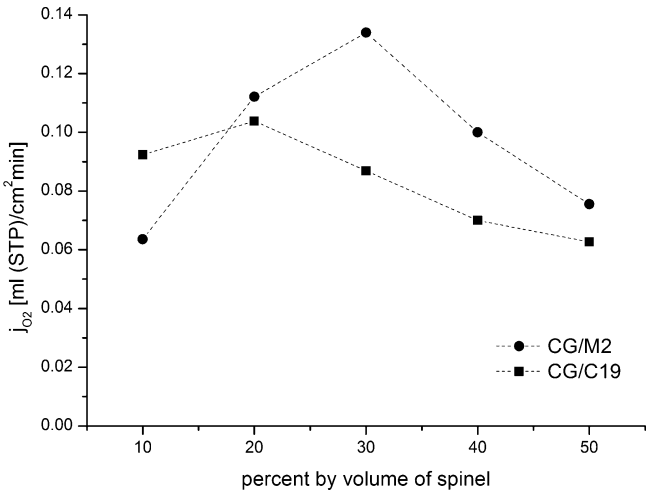

Fig. 7: Oxygen flux at 900 °C in an air/nitrogen gradient for both composite materials is plotted against the volume fraction of spinel.

Independent of the volume ratio of the composite composition, the absolute oxygen flux of CG/M2 ranges on a higher level compared to CG/C19. The oxygen fluxes of both materials are compared to the temperature range between 600 to 900 °C in Fig. 8 for a constant ECP volume fraction of 30 vol%.

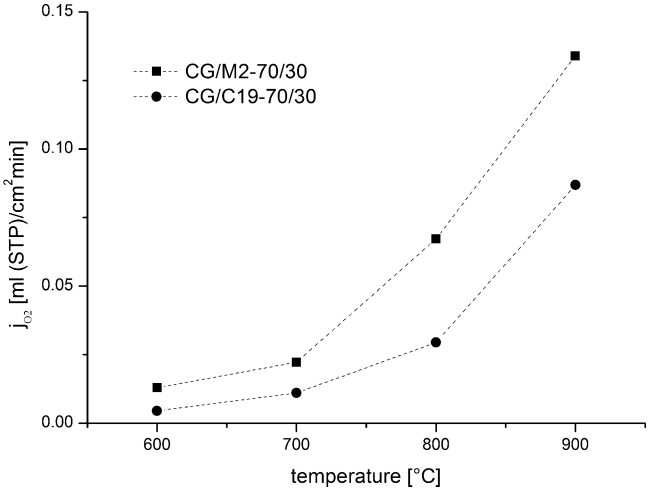

Fig. 8: Oxygen fluxes of CG/C19 – 70/30 and CG/M2 – 70/30 in a temperature range from 600 to 900 °C measured in an air/nitrogen gradient.

In addition to the heat treatment tests described below, the CO_2-stability of the two composite materials was tested in permeation experiments with CO_2 as sweep gas. The oxygen flux through the CG/M2 – 70/30 and CG/C19 – 70/30 samples vs. square root of time after switching from N_2 to CO_2 (900 °C) is shown in Fig. 9. The oxygen flux of both materials increases linearly with the square root of time up to 150 % of the initial value. In contrast, high-flux perovskite membrane materials usually demonstrate a sharp decrease of oxygen flux in the presence of CO_2 [5,12]. The linear regression of the oxygen fluxes to the square root of time results in correlation coefficients higher than 0.98. This behaviour indicates layer growth controlled by diffusion. Nevertheless,

verification of this assumption requires further investigations. Therefore, both samples were matted and roughened at the CO_2-exposed circular area for both materials. This was observed directly after the samples had cooled down to room temperature and been removed from the test rig. The sealing areas (ring areas covered by the tubular recipients) were unaffected and retained the shining appearance of a polished sample. The transition between both regions was abrupt and no intermediate section was found, indicating good performance of the sample sealing by clamping [12]. The polished feed gas side of the samples was only slightly affected and was covered by a thin light grey layer. A similar but much weaker matting effect was observed even for permeation tests in an air/nitrogen gradient.

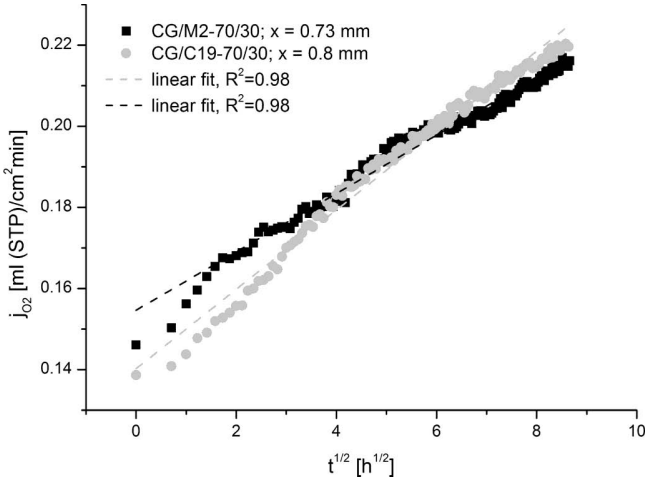

Fig. 9: Oxygen fluxes of CG/C19 – 70/30 and CG/M2 – 70/30 at 900 °C over the measurement time (75 h) determined in an air/CO_2 gradient.

SEM analyses were conducted to study the observed material degradation in detail. Different surfaces of a CG/M2 – 70/30 sample are shown in Fig. 10. The left part of Fig. 10 shows the unaffected sealing area after the sample run. In comparison to the left of Fig. 4, the material did not change its dual-phase structure. Both phases coexist separately and a small amount of residual closed porosity is visible.

The surface-exposed CO_2 is shown in the middle of Fig. 10. A porous, powder-like surface was formed and the former dual phase structure was completely destroyed. In the right part of Fig. 10 the feed-gas- or air-exposed surface is shown. The surface is covered with single solitaire crystallites. In both cases, incipient reactivity between the Mn of the spinel phase and the Ce-Gd-phase was found by means of EDX-analysis.

(5) Heat-treatment in model flue gas atmosphere

Scanning electron micrographs (SEM) show the surfaces of both composite materials before (left) and after the treatment in the model flue gas atmosphere at 850 °C with a dwell time of 24 h. As seen in Fig. 11, a very small change in the microstructure was observed. Nevertheless, the two phases (spinel grey and CG white) are still visible. The microstructure of the CG/C19 – 70/30 composite is almost unaltered as shown in Fig. 12.

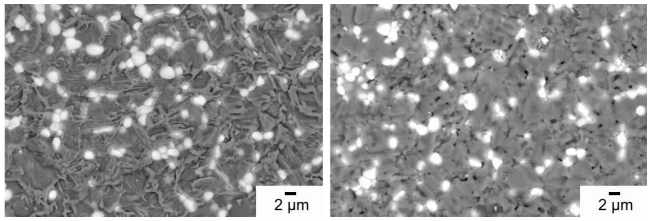

Fig. 11: SEM analysis of a CG/M2 – 70/30 bulk sample before (left) and after (right) an exposure test at 900 °C for 24 h under a CO_2-, SO_2-, O_2-containing model gas atmosphere.

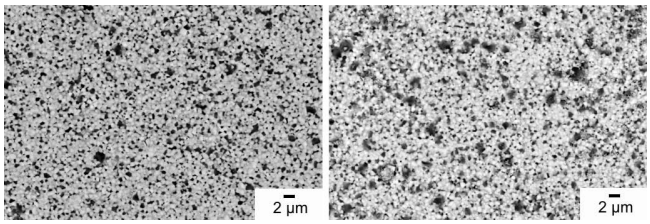

Fig. 12: SEM analysis of a CG/C19 – 70/30 bulk sample before (left) and after (right) an exposure test at 900 °C for 24 h under a CO_2-, SO_2-, O_2-containing model gas atmosphere.

The XRD patterns of the powder samples before and after the heat treatment experiments are compared in Fig. 13 for both 70/30 composites. Obviously, the heat-treatment in the model flue gas atmosphere did not cause the formation of foreign phases. For each composite material, the basic phases CG and spinel were unaffected by the treatment. Moreover, no indications of degradation by CO_2 and SO_2 were detected for powders as well as for bulk samples.

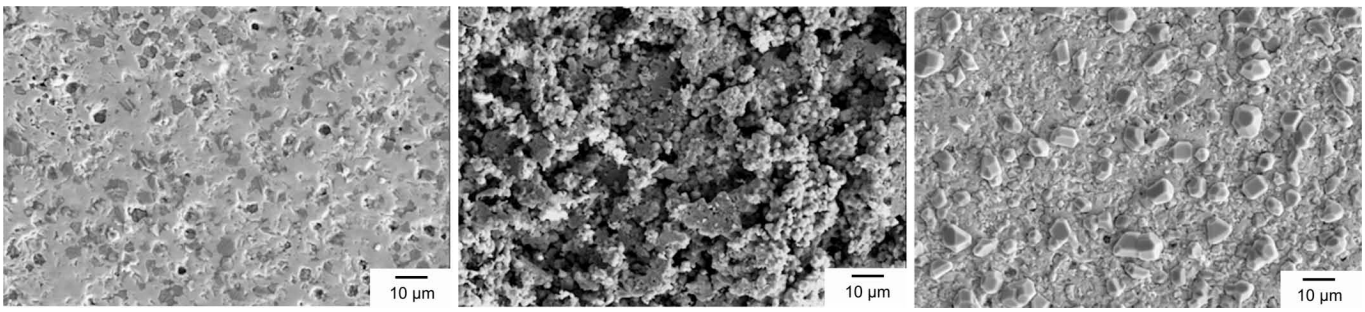

Fig. 10: SEM analysis of a CG/M2 – 70/30 sample after an oxygen permeation experiment at 900 °C in an air/CO_2 gradient, (left) unaffected sealing area, (middle) strongly roughened CO_2 exposed surface after the experiment, (right) slightly degraded feed gas side of the sample.

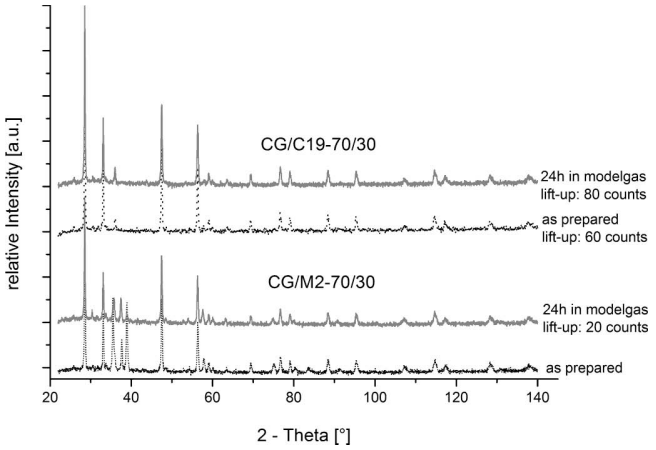

Fig. 13 : XRD patterns of powder samples of CG/C19 – 70/30 and CG/M2 – 70/30 before and after the exposure tests at 900 °C for 24 h under a CO_2-, SO_2-, O_2-containing model gas atmosphere.

IV. Discussion

A percolative conduction network required for an O_2-transporting dual-phase membrane can be realized with a conventional preparation route like the mixed oxide route. The majority of the compositions of an electronic conducting phase and an ionic conducting phase investigated so far react vigorously with one another already at lower temperatures, according to the reaction of Bi_2O_3 with silver and of doped CeO_2 with BSCF ($Ba_{0.5}Sr_{0.5}Co_{0.8}Fe_{0.2}O_{3-\delta}$) or other perovskites. In contrast to that it was shown that the phases of the examined composites are chemically stable in contact to each other for temperatures up to 1200 °C. In permeation measurements an optimal mixture of the CG and the spinel component of 70/30 for both composite materials was determined. Heat treatment of composite samples in a model flue gas at elevated temperature revealed that the dual-phase membranes are chemically stable in CO_2-and also in SO_2-containing atmospheres. SEM and XRD analyses of these samples demonstrated no significant material decomposition after treatment at 850 °C over a period between 5 and 24 h for composite powders and 24 h for the solid pellets. Beginning surface modifications were observed, indicating a possible degradation of the material stability.

In contrast to that, the results from oxygen permeation experiments conducted with CO_2 as sweep gas and air as feed gas clearly confirmed the material degradation. Depending on the orientation of the sample (sweep or feed side), a dramatic material decomposition as well as the formation of new reaction products owing to reactivity between mainly the Mn of the spinel phase and the CG-phase were found and proven by means of EDX spot analysis.

Nevertheless, the oxygen flux was affected in a positive manner by this material corrosion. An increase up to 150 % was observed. The expected blocking of the oxygen flux by the formation of carbonates and sulphates was not observed. These results suggest a surface activation effect of the corrosion products being formed like a porous catalytic layer as described in literature [18, 19, 20]. The formation of the corrosion products seems to be diffusion-controlled and can be described by a square-root-time dependence. Another possible explanation could be the kinetic demixing effect, a well-known and described mechanism for oxide solid solutions. Moreover, the kinetic demixing in an oxygen partial pressure gradient was described even for the two phase system wustite ((Mn, Fe)O)/spinel ((Mn, Fe)$_3O_4$) [21, 22, 23].

Comparing the material behaviour after the heat treatment in the model flue gas in contrast to the material decomposition under permeation conditions, the decomposition occurs more slowly even in an air/nitrogen gradient applied during the oxygen permeation measurement. Therefore, the impact of the corrosive gases seems to be negligible but the kinetic demixing probably always occurs.

The growth of a corrosion product layer was evident after only 75 h on the surface exposed to the sweep gas side of the investigated composite materials. In contrast, Lein *et.al.* [24] reported about a corrosion layer at the air side for LSCF ($La_{0.5}Sr_{0.5}Fe_{1-x}Co_xO_{3-\delta}$ with x = 0, 0.5 and 1). Further detailed investigations regarding this aging behaviour could be used to estimate the membrane thickness required for long-time operation without failure.

The thermal expansion coefficients of CG and the used spinels are much lower compared to mixed conducting perovskites and close to that of magnesia. The preparation of thin composite layers on an inert porous magnesia support seems promising if the required layer thickness for long-time operation is low enough for oxygen fluxes in a sufficiently high range.

V. Conclusions

An enhancement of the O_2 permeation is mandatory for the application of composite membranes in a technical plant. One possibility is the development of asymmetric membranes based on ceria composites because of their stability in flue gas atmosphere. Accordingly, different CG/spinel composites were synthesized with the solid state reaction route without phase transition effects. Heat-treatment in a CO_2-, O_2-, SO_2-containing model flue gas atmosphere demonstrated very promising stability for application in real flue gas. Permeation experiments revealed a strong kinetic demixing of the composites and the formation of corrosion layers on the surfaces of the samples exposed to the feed and sweep gas. This was accompanied by increasing oxygen fluxes, which might be due to surface activation by the corrosion products. According to a first approximation, the corrosion process follows a diffusion-controlled square-root-time dependence. Concerning the low oxygen fluxes, the industrial application of the investigated materials requires thin membranes, probably on an inert porous support such as magnesia. In further experiments, an optimum regarding both an adequate oxygen flux and a corrosion-resistant layer thickness has to be found. Furthermore, the observed corrosion processes should be clarified in detail for using the investigated CO_2- and SO_2-stable materials as asymmetric oxygen permeable membranes.

References

1 Federal Ministry of Economics and Labour, Germany, Research and Development Concept for Zero-Emission Fossil-Fuelled Power Plants. Summary of COORETEC (2003).

2 Fu, C., Gundersen, T.: Using exergy analysis to reduce power consumption in air separation units for oxy-combustion processes, *Energy*, **44**, 60 – 68, (2012).

3 Schulte, T., Waser, R., Römer, E.W.J., Bouwmeester, H.J.M., Nigge, U., Wiemhöfer, H.-D.: Development of oxygen-permeable ceramic membranes for NOx-sensors, *J. Eur. Ceram. Soc.*, **21**, 1971 – 1975, (2001).

4 Stadler, H., Beggel, F., Habermehl, M., Persigehl, B., Kneer, R., Modigell, M., Jeschke, P.: Oxyfuel coal combustion by efficient integration of oxygen transport membranes, *Int. J. Greenh. Gas Con.*, **5**, 7 – 15, (2011).

5 Arnold, M., Wang, H., Feldhoff, A.: Influence of CO_2 on the oxygen permeation performance and the microstructure of perovskite-type $(Ba_{0.5}Sr_{0.5})(Co_{0.8}Fe_{0.2})O_{3-\delta}$ membranes, *J. Membrane Sci.*, **293**, 44 – 52, (2007).

6 Bucher, E., Egger, S., Caraman, G., Sitte, W.: Stability of the SOFC cathode material $(Ba_{0.5}Sr_{0.5})(Co_{0.8}Fe_{0.2})O_{3-\delta}$ in CO_2-containing atmospheres, *J. Electrochem. Soc.*, **155**, B1218 – B1224, (2008).

7 Engels, S., Markus, T., Modigell, M., Singheiser, L.: Oxygen permeation and stability investigations on MIEC membrane materials under operating conditions for power plant processes, *J. Membrane Sci.*, **370**, 58 – 69, (2011).

8 Efimov, K., Klande, T., Juditzki, N., Feldhoff, A.: Ca-containing CO_2-tolerant perovskite materials for oxygen separation, *J. Membrane Sci.*, **389**, 205 – 215, (2012).

9 Zeng, Q., Zuo, Y.-B., Fan, G.-G., Chen, C.-S.: CO_2-tolerant oxygen separation membranes targeting CO_2 capture application, *J. Membrane Sci.*, **335**, 140 – 144, (2009)

10 Zhang, K., Ran, R., Ge, L., Shao, Z., Jin, W., Xu, N.: Systematic investigation on new $SrCo_{1-y}NbyO_{3-\delta}$ ceramic membranes with high oxygen semi-permeability, *J. Membrane Sci.*, **323**, 436 – 443, (2008).

11 Dong, X., Zhang, G., Liu, Z., Zhong, Z., Jin, W., Xu, N.: CO_2-tolerant mixed conducting oxide for catalytic membrane reactor, *J. Membrane Sci.*, **340**, 141 – 147, (2009).

12 Schulz, M., Kriegel, R., Kämpfer, A.: Assessment of CO_2 stability and oxygen flux of oxygen permeable membranes, *J. Membrane Sci.*, **378**, 10 – 17, (2011).

13 Megel, S., Girdauskaite, E., Sauchuk, V., Kusnezoff, M., Michaelis, A.: Area specific resistance of oxide scales grown on ferritic alloys for solid oxide fuel cell interconnects, *J. Power Sources*, **196**, 7136 – 7143, (2011).

14 Kriegel, R., Kircheisen, R., Töpfer, J.: Oxygen stoichiometry and expansion behavior of $Ba_{0.5}Sr_{0.5}Co_{0.8}Fe_{0.2}O_{3-\delta}$, *Solid State Ionics*, **181**, 64 – 70, (2010).

15 Waindich, A., Möbius, A., Müller, M.: Corrosion of $Ba_{1-x}Sr_xCo_{1-y}Fe_yO_{3-\delta}$ and $La_{0.3}Ba_{0.7}Co_{0.2}Fe_{0.8}O_{3-\delta}$ materials for oxygen separating membranes under oxycoal conditions, *J. Membrane Sci.*, **337**, 182 – 187, (2009).

16 Bunde, A., Roman, E.: Laws of disorder, (in German), *PhiuZ*, **27**, 246 – 256, (1996),

17 Lorenz, C.D., Ziff, R.M.: Precise determination of the bond percolation thresholds and finite-size scaling corrections for the sc, fcc, and bcc lattices, *Phys. Rev. E*, **57**, 230 – 236, (1998).

18 Pan, H., Li, L., Deng, X., Meng, B., Tan, X., Li, K.: Improvement of oxygen permeation in perovskite hollow fibre membranes by the enhanced surface exchange kinetics, *J. Membrane Sci.*, **428**, 198 – 204, (2013).

19 Tan, X., Wang, Z., Liu, H., Liu,S.: Enhancement of oxygen permeation through $La_{0.6}Sr_{0.4}Co_{0.2}Fe_{0.8}O_{3-\delta}$ hollow fibre membranes by surface modifications, (2013), **324**, 128 – 135, (2008).

20 Baumann, S., Serra, J.M., Lobera, P.M., Escolástico, S., Schulze-Küppers, F., Meulenberg, W.A.: Ultrahigh oxygen permeation flux through supported $Ba_{0.5}Sr_{0.5}Co_{0.8}Fe_{0.2}O_{3-\delta}$ membranes, *J. Membrane Sci.*, **377**, 198 – 205, (2011).

21 Petot-Ervas, G., Dufour, L.-C., Monty, C.: Dynamic segregation in multicomponent oxides under chemical potential gradients, *Nato. Adv. Sci. I E-App.*, **173**, 337 – 349, (1989).

22 Schmalzried, H.: Demixing, decomposition and degradation of oxides in chemical potential gradients, *Faraday Trans.*, **86**, 1273, (1990).

23 Ueshima, Y., Schmalzried, H., Koepke, J.: Demixing of oxide solid solutions in oxygen potential gradients: Two-phase systems and the morphological stability of the interface, *Solid State Ionics*, **40 – 41**, Part 1, 232 – 235, (1990).

24 Lein, H.L., Wiik, K., Grande, T.: Kinetic demixing and decomposition of oxygen permeable membranes, *Solid State Ionics*, **15**: Proceedings of the 15th International Conference on Solid State Ionics, Part I, **177**, 1587 – 1590, (2006).